Characterization of a membraneless direct-methanol micro fuel cell

I B Sprague[1], **P Dutta**[1,2*], and **S Ha**[3]
[1]School of Mechanical and Materials Engineering, Washington State University, Pullman, Washington, USA
[2]Department of Aerospace and Information Engineering, Konkuk University, Seoul, Republic of Korea
[3]School of Chemical Engineering and Bioengineering, Washington State University, Pullman, Washington, USA

The manuscript was received on 26 November 2008 and was accepted after revision for publication on 18 May 2009.

DOI: 10.1243/09576509JPE724

Abstract: The performance of a membraneless laminar flow micro fuel cell was evaluated under different operating conditions. The fuel cell was microfabricated in polydimethylsiloxane using standard soft-lithography techniques. It used methanol solution as the fuel for the anode side, and oxygen saturated sulphuric acid for the cathode. The parameters studied were the methanol concentration, flowrate, device width, and the concentration of sulphuric acid in the anode stream. Performance was characterized by V–I plots, stability of open circuit potential (OCP), polarization resistances, and anode polarization curves. We observed behaviour different from that shown thus far by existing laminar flow fuel cells. Our results show that the power output of the device decreases with an increase in the methanol concentration. An increase in the flowrate also decreases the power output of the device. It is shown that these trends are likely caused by the cell's internal resistance to proton transport. The addition of sulphuric acid to the fuel significantly decreases this resistance. It was found that the device OCP was not stable over extended operation, and could drop by more than 150 mV in 72 h.

Keywords: microfluidic fuel cell, membraneless, laminar flow, open circuit potential

1 INTRODUCTION

Demands for new sources of portable power have given rise to recent work on miniaturized fuel cell technology [**1**]. A promising direction is the development of fuel cells that use laminar flow to separate the fuel and oxidant streams. This eliminates the need for a membrane because the anode and cathode reactions are separated by laminar flow, but protons are still allowed to transport across the fluid–fluid interface. These laminar flow fuel cells (LF-FCs) are better suited for miniaturization because they require no membrane which leads to a simplified cell design compared to the conventional polymer electrolyte membrane (PEM) fuel cell [**1**]. The device cost is also reduced without the expensive proton exchange membrane.

The concept of a membraneless fuel cell was first demonstrated by Ferrigno *et al.* [**2**] with a vanadium redox fuel cell. Choban *et al.* [**3**] did the initial characterization study of LF-FCs using a direct formic acid cell and identified performance limiting factors such as reaction kinetics, fuel crossover, and reactant transport to the electrodes. Later, they concluded that poor oxygen replenishment at the cathode was the dominant limitation in LF-FC performance [**4**].

Bazylak *et al.* [**5**] studied the behaviour of a T-channel design numerically, focusing on the fuel utilization, which was shown to be poor. They proposed a tapered electrode design that would greatly increase fuel utilization and device performance. More analytic work was performed by Chang *et al.* [**6**] to study LF-FC behaviour of a Y-channel under different operating conditions. They showed that flowrate, channel geometry, and reactant concentrations all affect the cell performance and confirmed oxygen transport to the cathode as the dominant limitation. Cohen *et al.* [**7**] proposed a novel design for an LF-FC using laminar flow between parallel plates instead of flow side by side in a channel. This planar channel design significantly increased the electrode surface area and allowed for easier fabrication of fuel cell stacks and arrays. Chen *et al.* [**8**] performed an analytic study of the planar

*Corresponding author: Department of Mechanical and Materials, Washington State University, PO Box 642920, WA 99164-2920, Pullman, Washington, USA.
email: dutta@mail.wsu.edu

channel design and found that the device behaviour and performance were comparable to the Y-channel designs. They concluded that a better method for improving LF-FC performance is needed than merely increasing the electrode surface area.

In a membraneless LF-FC, the fuel/oxidizing agent selection is flexible. Hasegawa *et al.* [**9**] used this flexibility to explore new fuel possibilities. They used H_2O_2 in acidic and alkaline solutions as the fuel at the anode and oxidizing agent at the cathode, respectively. Cohen *et al.* [**10**] also demonstrated that LF-FCs can be operated with a different pH for the anode and cathode electrolytes to achieve significantly increased open circuit potential (OCP). Choban *et al.* [**11**] studied the effect of operating LF-FCs in all acidic, all alkaline, and acidic/alkaline conditions. Despite showing better performance they concluded that acidic/alkaline mixed operation is not a promising avenue because of a significantly lower theoretical maximum energy density than all acidic or all alkaline conditions.

In LF-FC, a lack of reactant replenishment at the cathode has been shown to be a large performance limitation because oxygen has a low concentration (2–4 mM) and diffusivity (2×10^{-5} cm^2/s) in an aqueous solution [**12**]. To improve the device performance, Jayashree *et al.* [**12**] presented an air-breathing LF-FC that uses a gas diffusion electrode at the cathode. This significantly reduced the oxygen transport limitation because of higher concentration (10 mM) and diffusivity (2×10^{-1} cm^2/s) of oxygen in air. Without the oxygen transport limitation, they were also able to show increased performance by operating in alkaline conditions because of improved anode kinetics [**13**].

Some recent work has looked at other aspects of LF-FCs. Lim *et al.* [**14**] studied the electrode diffusion layer, specifically the electrode's geometry effect on performance. Sun *et al.* [**15**] used a three-stream channel with a third electrolyte stream separating the anode and cathode streams to eliminate fuel crossover. Li *et al.* [**16**] demonstrated a simplified fabrication scheme and a fuel recycling system improving LF-FC's commercial possibilities.

The LF-FCs presented so far have had meso-scale channels with the smallest dimension being on the order of 0.5–1 mm. In order for LF-FCs to meet the power demands of portable power applications multiple cells will need to be stacked together. This means smaller (cell) channel sizes are needed to minimize the total volume of the stack. However, as they become microchannels, with the smallest dimension on the order of 1–10 μm, the operating behaviour may change. It is well known in the MEMS community that scaling effects can affect device behaviour in unexpected ways as surface effects and forces such as surface tension and viscous forces become dominant [**17**]. In this article we study an LF-FC that has a channel height of 10 μm to investigate if any performance changes arise in microscale. Moreover, the fuel source that has been predominantly studied in LF-FCs is formic acid. Methanol has a higher energy density over formic acid, which is a very important factor in portable power applications. Because of this we selected methanol as the fuel in this study. The long term performances of microfluidic-based direct methanol fuel cell are also presented for the suitability of this device.

2 EXPERIMENTAL SECTION

2.1 Materials and reagents

Pure methanol and sulphuric acid were purchased from Aldrich (St Louis, MO). Fluorescent dye, rhodium-*b*, was obtained from Acros (Morris Plains, NJ). Platinum black and platinum-ruthenium black (50:50 atomic per cent) were procured from Alfa Aesar (Ward Hill, MA). Nafion (5 per cent solution) was obtained from Solution Technology Inc (Mendenhall, PA).

2.2 Design of laminar flow fuel cell

The LF-FC was made with polydimethylsiloxane (PDMS) on a glass substrate. A schematic of the device and its operation principle are shown in Fig. 1. The dimensions of the straight microchannel are 10 μm tall and 25 mm long, while the width is either 1 mm or 3 mm. The branch channels of *Y*-junction are 10 μm tall, 150 μm wide, and 5 mm long. Each reservoir is 5 mm in diameter. The gold electrodes were deposited on both sides of the channel with dimensions of 20 mm long, 0.5 mm wide, and 375 nm thick. The anode and cathode catalysts are Pt–Ru Black and Pt Black, respectively. Pt–Ru was used at the anode to limit CO poisoning, which is a poisoning intermediate for methanol oxidation. Fuel, 0.5–4 M methanol solution, and oxidant, oxygen saturated sulphuric acid, were supplied through inlet reservoirs, while the waste, reaction by-products CO_2, water, and unutilized fuel, was collected in the exit reservoir.

2.3 Fabrication of the laminar flow fuel cell

The steps involved in fabricating the fuel cell are shown in Fig. 2. A positive mould was first made on a glass slide (Fig. 2(a)) using standard photolithographic techniques. Briefly, photoresist was spun on (Fig. 2(b)) and patterned using positive lithography (Figs 2 (c) and (d)). PDMS prepolymer and curing agent (Sylgard 184, Dow Corning Inc., Midland, MI) were mixed with a ratio of 10:1 and poured onto the mould. The PDMS was then degassed for 2 h at 0.001 Torr and baked at 80 °C for 3 h (Fig. 2 (e)). The PDMS channel was removed from the mould and trimmed to size. The reservoirs were formed using a 20 gauge

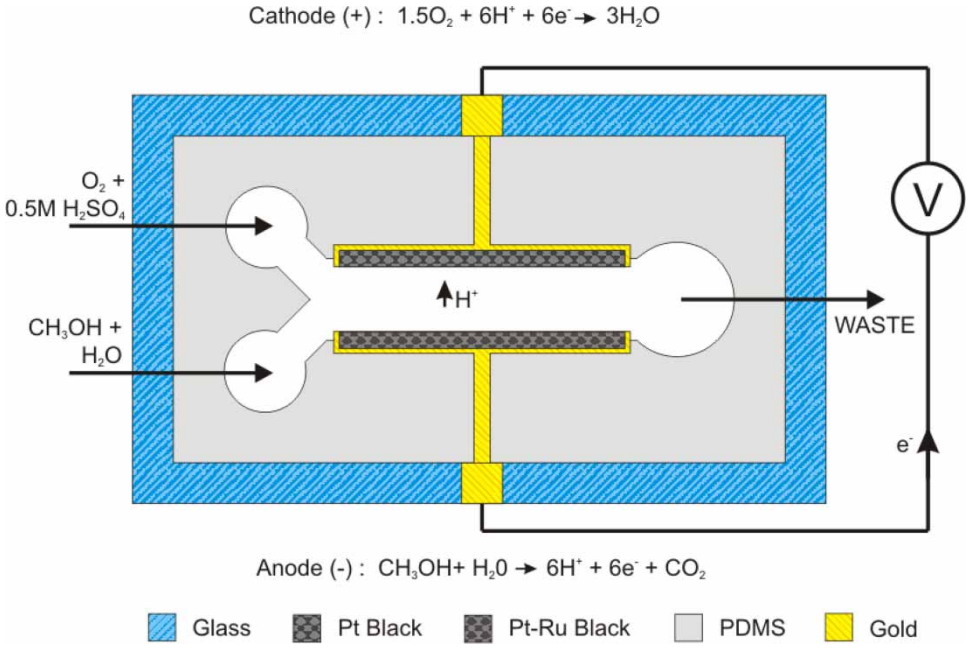

Fig. 1 Schematic of the LF-FC

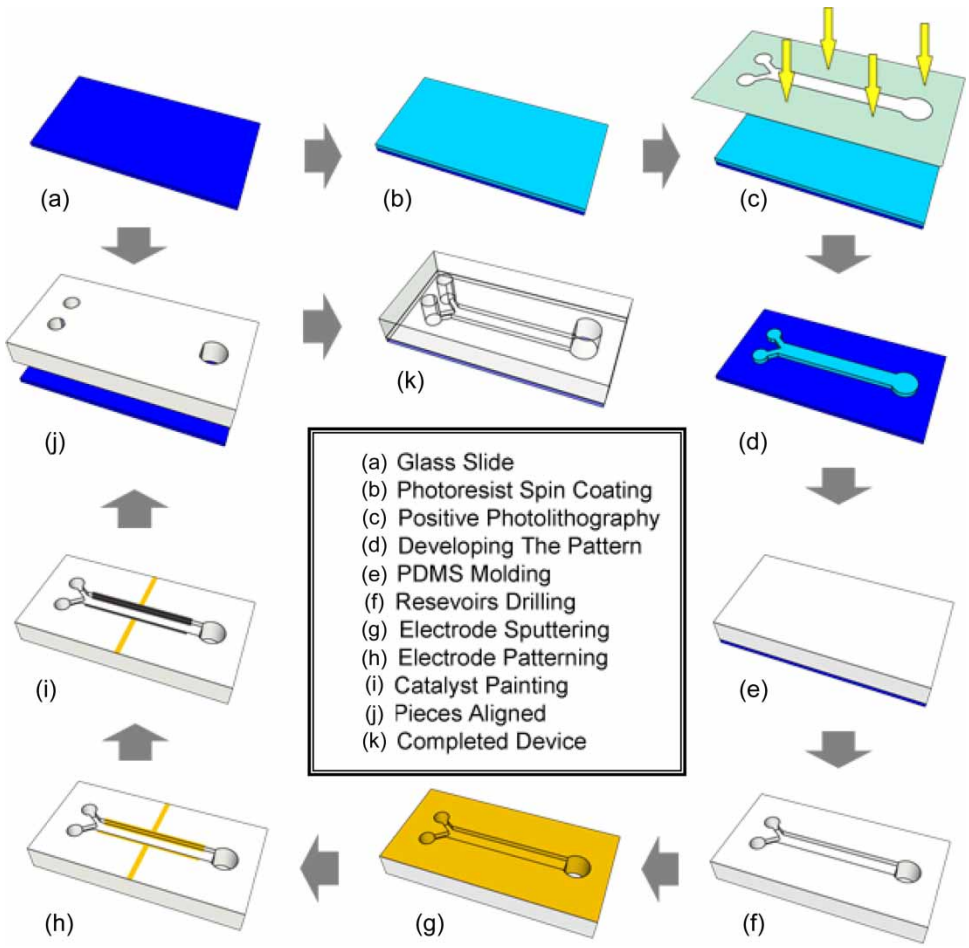

Fig. 2 Fabrication sequences of the LF-FC

needle to punch out holes in the PDMS (Fig. 2(f)). Next a thin layer of gold (375 nm) was sputtered using TiW film (10 nm) as an adhesion layer (Fig. 2(g)). The electrodes were then formed by standard gold patterning techniques (Fig. 2(h)). Catalyst inks were prepared by mixing appropriate amounts of catalyst particles,

Millipore water, and Nafion® solution. This mixture was sonicated and applied to the gold electrodes using a brush, and a heat lamp was used to evaporate the excess water (Fig. 2(i)). The PDMS channel was exposed to oxygen plasma and placed on a glass slide (Fig. 2(j)) using slight pressure and allowed to sit for 24 h creating a permanent bond and the final device (Fig. 2(k)). Capillary tubes were then glued in the reservoirs for transport of reactants and products to and from the device, respectively. Finally, wires were cold soldered using silver conductive epoxy (MG Chemicals, Burlington, Ontario) to form the electrical leads of the fuel cell.

2.4 Test of the fuel cell

First the fuel and oxidant solutions were prepared in the laboratory. For the fuel, pure methanol was diluted with Millipore water to the desired concentration. For the oxidant, oxygen saturated 0.5 M sulphuric acid was used. The oxygen was dissolved in the sulphuric acid by bubbling it for 30 min. These solutions were pumped through the device using a syringe pump (74900-10, Cole-Parmer Instrument Company, Vernon Hills, IL) at flowrates 1, 2, or 3 μL/min. In all tests, the flowrates of the anode and cathode streams were identical and equal to the flowrate specified by the operating conditions. Also, the cell was allowed to run for an hour for the flow to reach a steady state. The fuel cell was operated at 1 M methanol (fuel) concentration and at a reactant flowrate of 2 μL/min for all cases, unless stated otherwise.

For the voltage–current (V–I) curve a resistance decade box (380400, Extech Instruments, Waltham, MA) was used to apply the various loads. A multimeter (410, Extech instruments, Waltham, MA) was used to measure the voltage across the channel and a second multimeter (187, Fluke Corporation, Everett, WA) measured the current flowing in the circuit at each load. Before taking a data point for the V–I plot, the voltage and current were allowed to stabilize for 5 min at each load condition. In addition, to measure the hysteresis, both forward and backward scans were performed for each V–I curve.

To characterize the anode performance, the device was operated as a half cell and an anode polarization test was performed. The anode stream was fed with the methanol solution, while the cathode stream was fed with 0.5 M sulphuric acid with no oxygen. The cell was run for an hour to allow the flow to develop and reach a steady state. Then an incremental voltage was applied across the cell using a power supply (6033A, Hewlett Packard, Palo Alto, CA). The applied voltage was increased from 0 to 700 mV in 50 mV steps at 30 s intervals. The current in the circuit was measured with a multimeter (187, Fluke Corporation, Everett, WA). The fuel cell operating as a half-cell maintains the same anode reaction, while the cathode electrode serves as both the counter and reference electrodes. This means that the anode polarization test allows the measure of performance limitations associated with the anode electrode only.

3 RESULTS AND DISCUSSION

3.1 Methanol and oxygen crossover

In a fluidic system mixing of one stream into another cannot be prevented. If the species of one stream were to diffuse all the way from the fluid–fluid interface to the opposing electrode, the cell performance would be adversely affected. This is known as fuel crossover that creates mixed potentials, decreases cell efficiency, and could even deactivate the catalyst. Fortunately, the device design and operating parameters can be controlled so that fuel crossover can be prevented. To do this, the flowrates must be large enough so as not to allow enough time for the species to diffuse far enough for crossover to occur. The distance one stream will diffuse into the other is referred to as transverse diffuse broadening. The theoretical transverse diffusive broadening at a specific distance (x) along the channel is given by [**6**, **18**]

$$\delta(y) \propto \left(\frac{DHx}{U}\right)^{1/3} \tag{1}$$

where D is the diffusivity of the species, H is the channel height, and U is the average fluid velocity in the channel. In this study, we used a very low aspect ratio planar microchannel (10 μm high). Hence, the theoretical transverse diffusive broadening will be much smaller than the channel width as shown in Fig. 3(a). For instance, in our micro fuel cell, the transverse diffusive broadening at the exit ($x = 25$ mm) is 60.8 μm if the reactant flowrate is 1 μL/min. Thus, the fuel crossover can be prevented in our planar system because the species of one stream cannot diffuse far enough before being swept out of the device and into the waste.

To confirm the calculated results, the mixing phenomenon was observed experimentally. Figures 3(b) to (d) show fluorescent images taken at different Reynolds numbers between 0.011 and 0.033 in a 3 mm wide fuel cell. Fluorescent dye was fed to one side of the cell (stream 1) and water to the other (stream 2). The images were captured using a fluorescent imaging microscope (Lecia DMLB, Bartels and Stout Inc., Bellevue, WA). Because of the limited field of view of the microscope, the entire device could not be captured in a single image. Therefore a series of images was taken and stitched together afterwards. Because the flow was steady state, this method would not produce any inaccuracies. The catalyst layer and side walls can be seen in the images. Near the outlet of the main channel, the

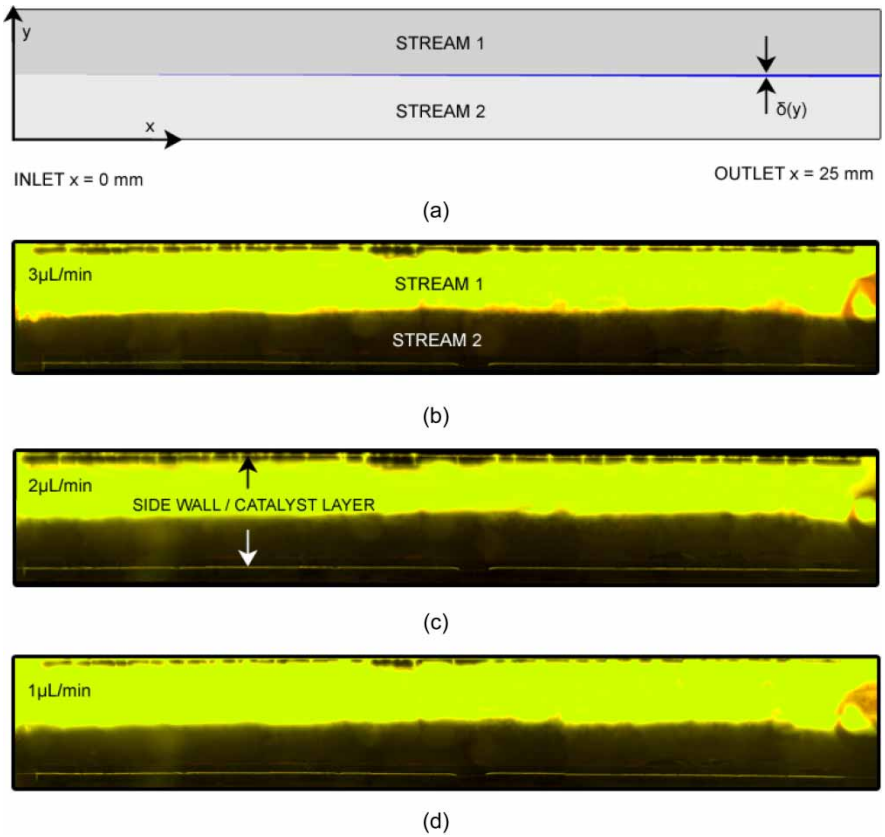

Fig. 3 (a) Theoretical transverse diffusive broadening along the channel. Fluorescent images of mixing of two streams in the main channel at Reynolds numbers of (b) 0.033, (c) 0.022, and (d) 0.011. Rhodium-*b* was used as the dye in stream 1 to show the amount of mixing into stream 2. The channel was 3 mm wide and 10 μm high

image is obscured by interference from the glue that was used for connecting outside capillary tubes.

From the theoretical calculations, it was unexpected that the fluorescent dye would diffuse a noticeable amount into the clear water for any of the Reynolds numbers studied. The fluorescent images confirm this as there appears to be very little mixing at the interface and that the fluorescent dye has not travelled across the channel a significant amount. In fact, there is little discernable difference in the mixing between the various Reynolds numbers. The three Reynolds numbers presented in Figs 3(b) to (d) confirm that the mixing zone is very small relative to the channel width and crossover is not an issue for this device.

3.2 Fuel concentration

Previous work has shown that the dominant performance limitation in LF-FC is oxygen transport to the cathode. Thus, for constant conditions at the cathode, increasing the fuel concentration to the anode has shown a limited effect on cell performance [**3**, **4**, **6**]. However, in this work, we observed a significant performance dependence on fuel concentration. Figure 4 shows the *V*–*I* curves for different methanol concentrations between 0.5 and 4 M.

The experimental results show that the fuel cell performance decreases as the methanol concentration increases. Clearly, this trend will not hold as the fuel concentration goes to zero as this would produce no performance. However, for the device presented, only a very small amount of fuel is required to yield comparable performance. This is very clear from the inset Fig. 4, where *V*–*I* plot (symbols) presented is for the case when the cell was initially fed with a 2 M methanol stream followed by stream of Millipore water. The performance data were taken while water was flowing through the device and the only fuel present is the residual fuel left along the side walls of the channel from the original fuel stream. The *V*–*I* plot (solid line) of 0.5 M case is also shown to compare the performances. Experimental results show that a very similar slope, which is equivalent to the polarization resistance of the cell, exists for both cases. Hence, although the overall potentials are lower, the cell resistance is essentially equivalent to the 0.5 M case, showing that the performance trend holds even for trace amount of fuel.

The performance shown in Fig. 4 is on the low end of results published for studies of similar devices. Choban *et al.* [**3**] demonstrated similar *V*–*I* plots with a device using formic acid as the fuel and potassium

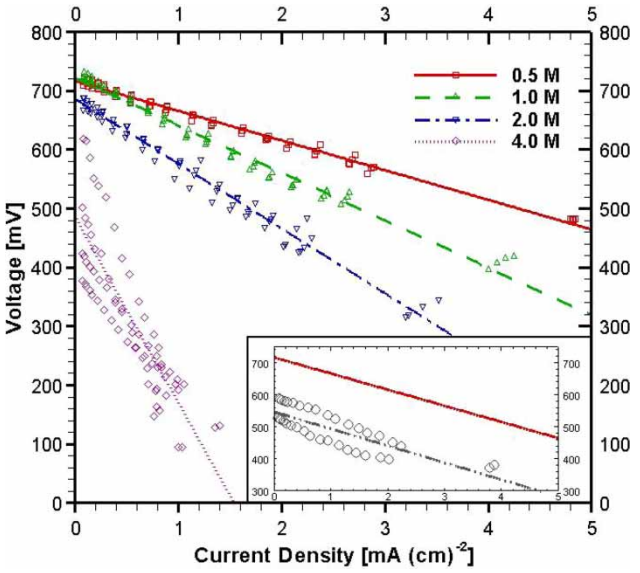

Fig. 4 Performance of the LF-FC operating at different methanol concentrations

permanganate as the oxidant. Choban *et al.* [**4**] characterized a direct methanol device with oxygen saturated sulphuric acid as the oxidant and achieved slightly better current densities but they used a mesoscale channel in their device. Other works on LF-FCs [**12**, **13**] have used an air breathing cathode to achieve an order of magnitude greater performance. However, this air breathing cathode presents major challenges if one would like to scale down the device to true microscale.

Figure 5(a) is a half-cell test of the anode with respect to methanol concentration and it illustrates the activity in the anode side based on fuel consumption. The decreased performance with increased methanol concentration can be attributed to a change in performance on the anode side of the cell (Fig. 5(a)). There are four possible reasons to explain this decreasing trend in performance at the higher methanol concentrations:

(a) methanol crossover creating mixed potential at the cathode;
(b) decreased anode kinetics;
(c) increased methanol transport resistance at the anode;
(d) increased Ohmic resistance.

As discussed above, fuel crossover is not present at all in the planar cell, and therefore, cannot be the cause of our performance drop with the higher methanol concentrations. The decreased anode kinetics also cannot be the reason because the electro-oxidation of methanol on Pt–Ru catalyst has a positive reaction order between 0.5 and 1 [**19**]. This means, the activity at the anode electrode should increase as the concentration of fuel increases. Therefore, the anode is not limited by kinetic performance with the higher methanol concentrations. Also, mass transport resistance should

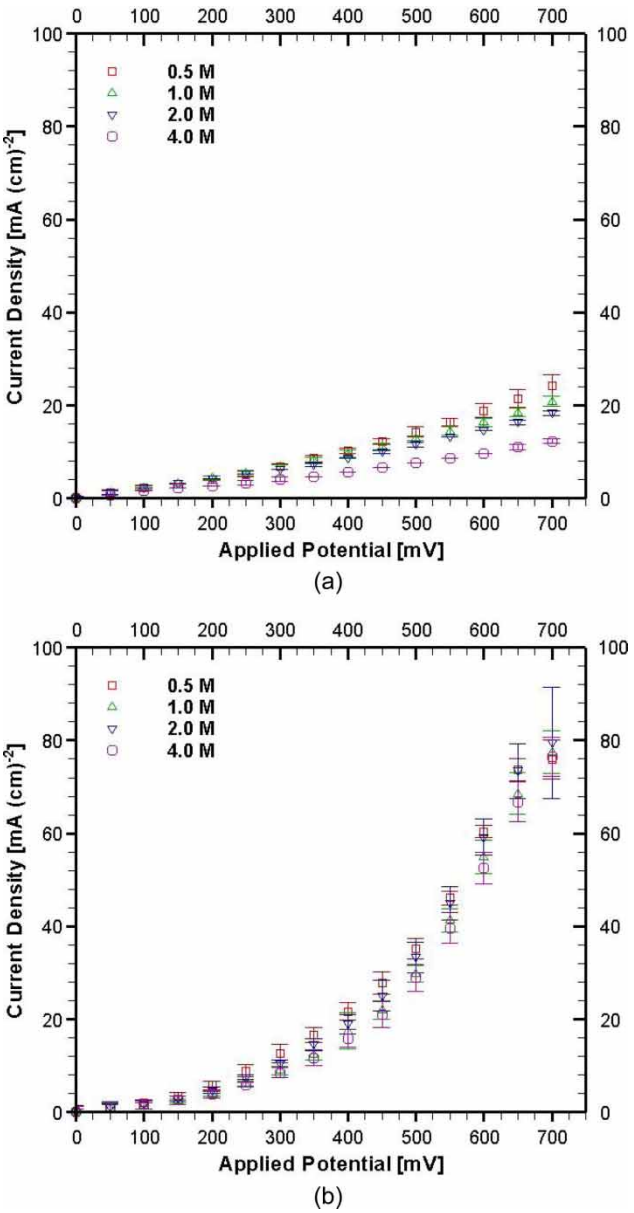

Fig. 5 Anode half-cell test. The effect of methanol concentration on anode performance for (a) methanol and (b) methanol with 0.5 M sulphuric acid

actually decrease with increased methanol concentration. This is because a higher concentration would create a higher driving force for the methanol to diffuse across the depletion boundary layer to the electrode. This leaves an increase in Ohmic resistance, the internal device resistance to ion (proton) conduction across the flowing electrolyte streams, as the only explanation for having decreased cell performance with the higher methanol concentrations.

Having a proper proton transport from the anode to cathode is essential in order to achieve a high cell performance. If the Ohmic resistance of the cell increases, the protons cannot be transported efficiently and this leads to a poor cell performance.

Protons are transported within the electrolyte by three means: migration, diffusion, and advection. The advective transport is because of the bulk flow of the electrolyte causing the ions to be transported with the flow. The Reynolds number in our channel is <1, and in the creeping flow regime there is no advection in the cross stream direction. Thus, advection in the cross stream direction cannot be used to explain the decreasing trend in the cell performance at higher methanol concentration. Previous works have cited diffusion as the primary mode of proton transport; however, for our cell this is not the case. Sulphuric acid is supplied to the cathode, which carries a lot of free protons. This supplied concentration of protons at the cathode will alter the concentration gradient, which is the driving force for diffusion. The concentration gradient can be calculated using the dissociation constants for sulphuric acid. Assuming 0.5 M sulphuric acid completely dissociates to its first protons and its second dissociation constant is $k_{a2} = 1.3 \times 10^{-2}$, the concentration of protons in the bulk cathode stream is on the order of 0.5 M. On the other hand, the concentration of protons produced by methanol oxidation at the anode can be calculated by relating current, Faraday's constant, and the number of protons produced per electron in methanol oxidation. Assuming the maximum current in our system, the concentration of proton produced at the anode is on the order of 0.01 M. There is an order of magnitude greater concentration of proton in the cathode than in the anode. This means that protons, along with SO_4^-, will then actually diffuse in the direction of the cathode to anode. Therefore, diffusion is not the cause of proton transport from the anode to the cathode, and cannot be the cause of the decreased performance at higher methanol concentrations. Clearly then, migration is the primary mode of transport of the protons from the anode to cathode in our cell. The anode reaction creates protons and the cathode reaction consumes them; therefore, there is a local net positive and negatives charges developed, respectively. This induced potential causes the migration of the protons.

The decreased performance in our cell as shown in Fig. 4 can then be explained in terms of an increased resistance to proton migration across the cell. Electromigration is proportional to the mobility of the ion in the electrolyte and the electric field strength. According to the Nernst equation, the theoretical cell potential will increase as the concentration of methanol increases. Thus, the change in electric field because of the higher methanol concentration cannot explain the decreasing trend in the cell performance that we observed in Fig. 4. Protons in pure water have a high mobility (about seven times greater than other positive ions). However, its high mobility decreases significantly with addition of a non-aqueous solvent, such as methanol. For instance, at 0.5 M methanol solution, the proton mobility is about 3.6×10^{-3} ($cm^2/(s \cdot V)$) and at 4 M methanol solution, the proton mobility decreases to about 2.7×10^{-3} ($cm^2/(s \cdot V)$) [**20**]. Therefore, as the methanol concentration increases, the proton mobility in the anode electrolyte stream decreases and the proton transport resistance increases. This increased resistance to proton transport from the anode to the cathode stream results in limited anode activity because methanol oxidation is slowed by the poor proton transport rate. By adding 0.5 M sulphuric acid to the anode stream, the overall proton conductivity of the anode stream increases. Figure 5(b) shows a half-cell test of the anode for different methanol concentrations with 0.5 M sulphuric acid added to the fuel solution. According to Fig. 5(b), there is no statistically significant effect of methanol concentration on anode activity. Also, an overall increase in methanol oxidation activity can be seen from the case with sulphuric acid comparing to the case without the sulphuric acid. This increase in activity can be explained by the decrease in resistance to proton transport. This proton transport limitation has not been shown in earlier works in part because the cells studied have primarily used formic acid as the fuel that has excellent proton mobility and thus a limited resistance to the proton transport.

3.3 Flowrate

Reactant flowrate should also have an influence on the device performance. The flowrate affects reactant replenishment at the electrodes and residence time for the reaction to occur. Previous works have shown that increased flowrate improves performance by increasing the reactant flux and decreasing the concentration boundary layer thickness providing better reactant supply to the electrodes [**3**]. Figure 6 shows *V–I* curves for our fuel cell as flowrate (Reynolds number) is increased from 1 μL/min ($Re = 0.011$) to 3 μL/min ($Re = 0.033$). Our experimental results suggest that the performance decreases with increasing flowrates yielding lower current densities at equivalent cell potentials. However, this trend will not hold true down to zero flowrate as this would yield no performance. Hence, there must be an optimal flowrate for any microscale fuel cell device to produce maximum power. In this study, we were not able to evaluate the performance at flowrates <1 μL/min because of the limitation of the pump used for this experiment. Nevertheless, the experimental study suggests that performances degrade at higher flowrates.

Figure 7(a) is a half-cell test showing the effect of reactant flowrate (Reynolds number) on anode performance in a 3 mm wide fuel cell. It can be seen that the decreased cell performance can be partially attributed to the decreased anode performance at the higher flowrates. There are two possible reasons for performance decrease at the higher flowrates:

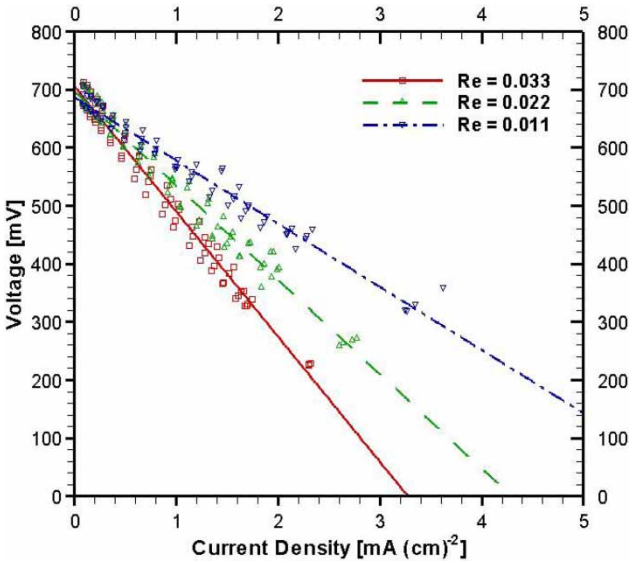

Fig. 6 Performance of the LF-FC operating at different reactant flowrates. The Reynolds number corresponding to flowrates of 1, 2, and 3 μL/min are 0.011, 0.022, and 0.033, respectively

shorter residence time and increased Ohmic losses. The residence time of methanol in our cell decreases from 18 to 8 s as the flowrate increases from 1 to 3 μL/min. However, the residence time of 8 s is still significantly higher than the residence times needed for methanol oxidation to occur. Therefore, we believe that the decrease in residence time is not the main reason for having the decreased cell performance with the higher flowrates (Reynolds numbers). Figure 7(b) shows a half-cell test for the above mentioned case with 0.5 M sulphuric acid added to the anode stream. It can be seen that the overall anode activity increases significantly and the performance is no longer a strong function of flowrate. Based on Fig. 7(b), we argue that the performance loss at higher flowrates (Reynolds number) is mostly caused by an increase in the Ohmic resistance. However, this flowrate effect on the cell performance needs additional investigations in the future to have a more comprehensive understanding.

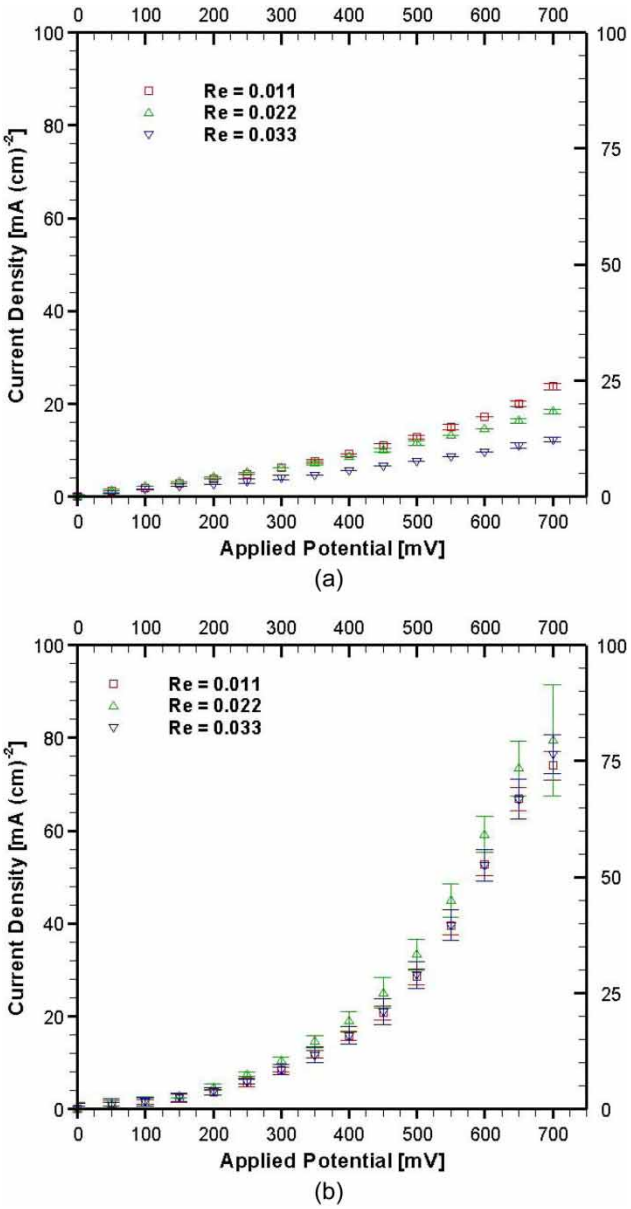

Fig. 7 Anode half-cell test. The effect of reactant flowrate on anode performance for (a) methanol and (b) methanol with 0.5 M sulphuric acid

3.4 Device size

The width of flow cell is very important in the performance study of micro fuel cell as hydrogen ions have to migrate from one electrode to the other to produce useful work. To demonstrate the effect of channel width, a second device with a channel width of 1 mm was fabricated and characterized. The cell polarization resistance is presented in Fig. 8 as a function of Reynolds number for both devices (channel width = 3 mm (Fig. 8(a)) and 1 mm (Fig. 8(b))) for different fuel concentrations. The cell polarization resistance is a measure of the cell's internal performance limitations and is equivalent to the negative of the slope of the V–I plot. The higher the cell resistance, the poorer the cell performance. The data show that the performance trends observed before (3 mm wide microchannel) also exist in the narrower (1 mm wide) microchannel device. However, the cell resistance decreases as we shrink the channel width. In other words, the cell performance improves significantly for a narrower channel. This is due to the fact that the total electrolyte resistance to proton conduction decreases as the distance between two electrodes decreases. One might expect even better performance at a much smaller channel width. However, we were not able to obtain reliable and repeatable results at channel width <1 mm because of technological limitation of the existing catalyst deposition process at both the anode and cathode sides.

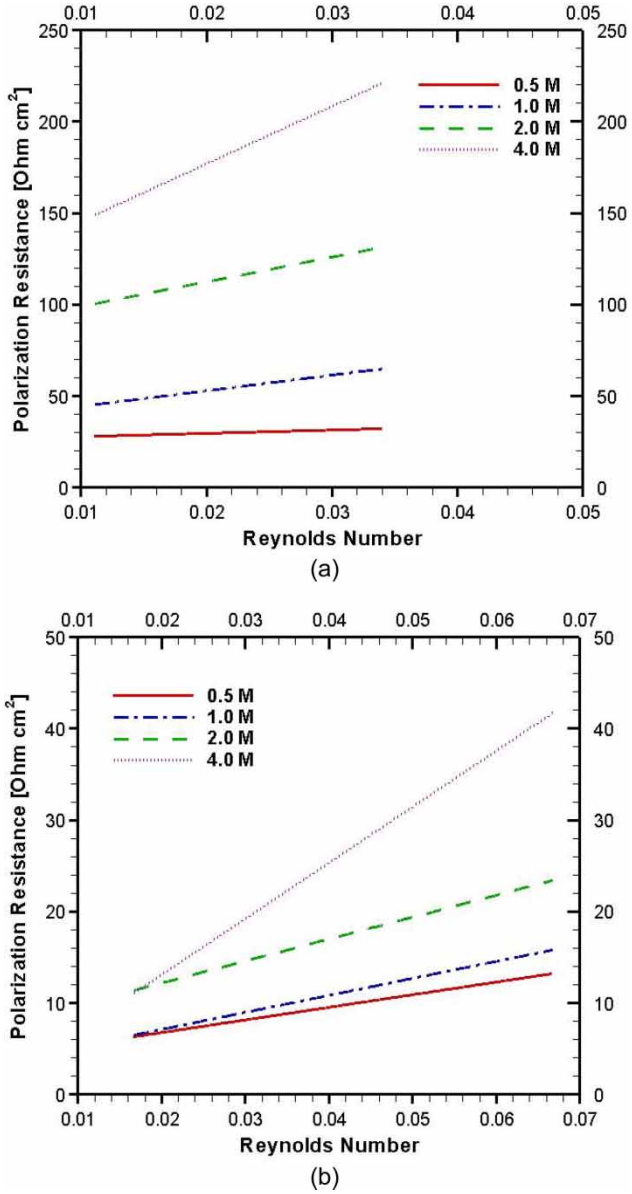

Fig. 8 Polarization resistance of fuel cell for (a) 3 mm wide and (b) 1 mm wide channels as a function of Reynolds number for different fuel concentrations. A planar microchannel was used to evaluate the performance of the micro fuel cell. Hence, the effect of channel width was not apparent in the flow Reynolds number

3.5 Stability

An important device characteristic that has not been studied in LF-FCs is the long-term stability. Although the stability of current at a fixed voltage is the standard measure of stability, we did not have the sufficient equipment to study this. The stability we considered was how the OCP changed with extended device operation time. It is interesting to note that for regular fuel cells the OCP tends to fluctuate, but in our device the change in OCP was a smooth (no fluctuation) decrease with time. To measure this stability, the device was operated at an open circuit for a long duration of time and the OCP was recorded as a function of time. For this experiment, the cell was fed with 1 M methanol solution to the anode and oxygen saturated sulphuric acid to the cathode and allowed to run constantly for 71 h. Figure 9 shows that the OCP behaviour over time. The cell took about an hour to develop the steady-state flow and reached the peak OCP of 700 mV. Then, the OCP began to decrease, initially the rate at which it drops is rather quick, but as time increases it dropped less rapidly. Although the rate of decent of the OCP slows down, the OCP never stabilizes to a steady-state value. This drop is either caused by the device degradation or some phenomenon in the device operation. At the 71 h, the fuel and oxidant flow were stopped and both the anode and cathode were fed with Millipore water. Water was fed to the device for 12 h which flushed out the cell, allowing it to be restarted. By restarting a flushed out device it can be determined if the OCP drop is caused by device degradation or by an operational characteristic. At the 83 h, 1 M methanol solution and oxygen saturated sulphuric acid were again fed to the anode and cathode, respectively. The device was run for another 36 h while OCP was again monitored. The magnitude and behaviour of the OCP is equivalent to the original 36 h. It can be concluded that the device had not degraded and that there is an operational phenomenon in LF-FCs that causes the OCP to drop. One explanation that applies to this same trend in regular macro scale PEM fuel cells is catalyst poisoning because of CO by-product of methanol oxidation. However, we used the bimetallic catalyst Pt–Ru specifically to limit this. Also, at OCPs, there is very little current draw generating very little CO intermediate, so catalyst poisoning is most likely not the cause. Further investigation would be required before definite phenomena could be cited as the cause for the instability in our LF-FC.

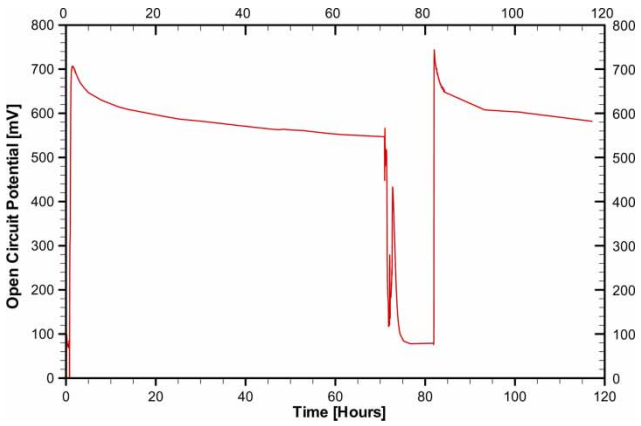

Fig. 9 Long term study of OCP of the LF-FC

4 CONCLUSIONS

A microscale LF-FC was fabricated on PDMS and its operating behaviour characterized. Standard microfabrication techniques were used to create the device. It was operated as a direct methanol fuel cell with oxygen saturated sulphuric acid as the oxidant. The effects of flowrates of the fuel and oxidizing agents, concentrations of methanol, and channel width were evaluated. The performance was characterized by V–I curves and anode polarization plots. The power output of the cell decreased as we increased the concentration of methanol supplied to the anode. This performance drop at the higher methanol concentration is mainly because of the increase in the proton transport resistance in the electrolyte system with higher methanol concentration. The power output also decreased as the flowrate of the fuel and oxidizing agents increased. We observed that the addition of sulphuric acid significantly improves the performance of LF-FCs at the higher methanol concentrations or higher flowrates by decreasing the resistance to proton transport. Furthermore, for a particular operating condition (such as flowrate, fuel concentration, and so on), the performance of fuel cell was much better for narrower channel width.

It was also found that the device OCP is not stable over extended operation. The device potential dropped over 150 mV in 72 h of continuous operation. It was shown that the cell could be flushed, restarted, and the same OCP curve could be obtained. We concluded that the cause of this potential drop over long durations of time is, therefore, not caused by the permanent cell degradation with use. Instead, it is related to a behavioural characteristic of LF-FC operation. Future work would need to address the device instability phenomenon more specifically.

The performance of our microscale fuel cell was inferior than that of a conventional fuel cell. Despite that fact, devices like this show promise in portable power applications because of their miniature sizes and simplicity of fabrication. However, before they can be fairly compared to established fuel cell technology, the performance characteristics of LF-FCs must be adequately understood through studies such as this one, which will allow for optimized device design.

REFERENCES

1 **Morse, J. D.** Micro-fuel cell power sources. *Int. J. Energy Res.*, 2007, **31**, 576–602.

2 **Ferrigno, R., Stroock, A. D., Clark, T. D., Mayer, M.,** and **Whitesides, G. M.** Membraneless Vanadium redox fuel cell using laminar flow. *J. Am. Chem. Soc.*, 2002, **124,** 12930–12931.

3 **Choban, E. R., Waszczuk, P., Markoski, L. J., Wieckowski, A.,** and **Kenis P. J. A.** Microfluidic fuel cell based on laminar flow. *J. Power Sources*, 2004, **128,** 54–60.

4 **Choban E. R., Waszczuk, P.,** and **Kenis, P. J. A.** Characterization of limiting factors in laminar flow-based membraneless microfuel cells. *Electrochem. Solid-State Lett.*, 2005, **8**(7), A348–A352.

5 **Bazylak, A., Sinton, D.,** and **Djilali, N.** Improved fuel utilization in microfluidic fuel cells: a computational study. *J. Power Sources*, 2005, **143,** 57–66.

6 **Chang, M., Chen, F.,** and **Fang, N.** Analysis of membraneless fuel cell using laminar flow in a Y-shaped microchannel. *J. Power Sources*, 2006, **159,** 810–816.

7 **Cohen, J. L., Westly, D. A., Pechenik, A.,** and **Abruna, H. D.** Fabrication and preliminary testing of a planar membraneless microchannel. *J. Power Sources*, 2005, **139,** 96–105.

8 **Chen, F., Chang, M. H.,** and **Lin, M. K.** Analysis of membraneless formic acid microfuel cell using a planar microchannel. *Electrochim. Acta*, 2007, **52,** 2506–2514.

9 **Hasegawa, S., Shimotani, K., Kishi, K.,** and **Watanabe, H.** Electricity generation from decomposition of hydrogen peroxide. *Electrochem. Solid-State Lett.*, 2005, **8**(2), A119–A121.

10 **Cohen, J. L., Volpe, D. J., Westly, D. A., Pechenik, A.,** and **Abruna, H. D.** A dual electrolyte H_2/O_2 planar membraneless microchannel fuel cell system with open circuit potentials in excess of 1.4 V. *Langmuir*, 2005, **21,** 3544–3550.

11 **Choban, E. R., Spendelow, J. S., Gancs, L., Wieckowski, A.,** and **Kenis, P. J. A.** Membraneless laminar flow-based micro fuel cells operation in alkaline acidic and acidic/alkaline media. *Electrochim. Acta*, 2005, **50**, 5390–5398.

12 **Jayashree, R. S., Gancs, L., Choban, E. R., Primak, A., Natarajan, D., Markoski, L. J.,** and **Kenis, P. J. A.** Air-breathing laminar flow-based microfluidic fuel cell. *J. Am. Chem. Soc.*, 2005, **127**, 16758–16759.

13 **Jayashree, R. S., Egas, D., Spendelow, J. S., Natarajan, D., Markoski, L. J.,** and **Kenis, P. J. A.** Air-breathing laminar flow-based direct methanol fuel cell with alkaline electrolyte. *Electrochem. Solid-State Lett.*, 2006, **9**(5), A252–A256.

14 **Lim, K. G., Tayhas, G.,** and **Palmore, R.** Microfluidic biofuel cells: the influence of electrode diffusion layer on performance. *Biosens. Bioelectron.*, 2007, **22**, 941–947.

15 **Sun, M. H., Casquilas, G. V., Guo, S. S., Shi, J., Ji, H., Ouyang, Q.,** and **Chen, Y.** Characterization of microfluidic fuel cell based on multiple laminar flow. *Microelectron. Eng.*, 2007, **84**, 1182–1185.

16 **Li, A., Chan, S. H.,** and **Nguyen, N.** A laser-micromachined polymeric membraneless fuel cell. *J. Micromech. Microeng.*, 2007, **17**, 1107–1113.

17 **Allen, J. J.** *Micro electro mechanical system design*, pp. 115–148 (Taylor & Francis Group, Boca Raton).

18 **Ismagilov, R. F., Stroock, A. D., Kenis, P. J. A.,** and **Whitesides, G.** Exeperimental and theoretical scaling laws for transverse diffusive broadening in two-phase laminar flows in microchannels. *Appl. Phys. Lett.*, 2000, **76**, 2376–2378.

19 **Vidakovic, T., Christov, M.,** and **Sundmacher, K.** Rate expression for electrochemical oxidation of methanol on a direct methanol fuel cell anode. *J. Electroanal. Chem.*, 2005, **580**, 105–121.

20 **Bockris, J.** and **Reddy, A. K. N.** *Modern electrochemistry: an introduction to an interdisciplinary area*, 1970, pp. 470–474 (Plenum Press, New York).